

# Shapes of stellar activity cycles

T. Willamo<sup>1</sup>, T. Hackman<sup>1</sup>, J. J. Lehtinen<sup>2</sup>, M. J. Käpylä<sup>3,2</sup>, N. Olsper<sup>2</sup>, M. Viviani<sup>2</sup>, and J. Warnecke<sup>2</sup>

<sup>1</sup> Department of Physics, P.O. Box 64, FI-00014 University of Helsinki, Finland  
e-mail: teemu.willamo@helsinki.fi

<sup>2</sup> Max Planck Institute for Solar System Research, Justus-von-Liebig-Weg 3, D-37077 Göttingen, Germany

<sup>3</sup> Department of Computer Science, Aalto University, PO Box 15400, FI-00076 Aalto, Finland

Received Month XX, XXXX; accepted Month YY, YYYY

## ABSTRACT

**Context.** Magnetic activity cycles are an important phenomenon in both the Sun and other stars. The shape of the solar cycle is commonly characterised by a fast rise and a slower decline, but not much attention has been paid to the shape of cycles in other stars.

**Aims.** Our aim is to study whether the asymmetric shape of the solar cycle is common in other stars as well, and compare the cycle asymmetry to other stellar parameters. We also study the differences in the shape of the solar cycle, depending on what activity indicator is used. The observations are also compared to simulated activity cycles.

**Methods.** We use the chromospheric Ca II H&K data from the Mount Wilson Observatory HK Project. From this data set we identify 47 individual cycles from 18 stars. We use the statistical skewness of a cycle as a measure of its asymmetry, and compare this to other stellar parameters. A similar analysis has been done to magnetic cycles extracted from direct numerical magnetohydrodynamic simulations of solar-type convection zones.

**Results.** The shape of the solar cycle (fast rise and slower decline) is common in other stars as well, although the Sun seems to have particularly asymmetric cycles. Cycle-to-cycle variations are large, but the average shape of a cycle is still fairly well represented by a sinusoid, although this does not take its asymmetry into account. We find only slight correlations between the cycle asymmetry and other stellar parameters. There are large differences in the shape of the solar cycle, depending on what activity indicator is used. In the simulated cycles, there is a difference in the symmetry of global simulations covering the full longitudinal range, hence capable of exciting non-axisymmetric dynamo modes, versus wedge simulations covering a partial extent in longitude, where only axisymmetric modes are possible. The former produce preferentially positive skewness, while the latter a negative one.

**Key words.** Stars: activity – Stars: chromospheres – Sun: activity

## 1. Introduction

The shape of the 11 year sunspot cycle is not perfectly symmetric, but characterised by a faster rise from minimum to maximum and slower decline from maximum to minimum (Waldmeier 1935). Another common feature, deviating from a sinusoid shaped cycle, is the typical double peak, known as the Gnevyshev gap (Gnevyshev 1963). Gnevyshev (1967, 1977) suggested that the solar cycle generally consists of two waves of activity. There is an asymmetry in solar activity between the northern and southern hemisphere (e.g. Newton & Milsom 1955; Deng et al. 2016). Norton & Gallagher (2010) studied the solar cycle separately on each hemisphere and concluded that differences in the hemispheres cannot explain the Gnevyshev gap, but there must be a mechanism producing it for both hemispheres. One factor which might affect it is the complexity of active regions. Simple active regions, with unipolar or bipolar sunspot groups, appear on average earlier in the solar cycle than more complex active regions (Nikbakhsh et al. 2019). Thus the simple regions dominate the first peak of the maximum, and the complex regions only have a notable effect on the latter peak. Feminella & Storini (1997) found that the activity dip in the Gnevyshev gap is more evident in high energy phenomena, such as the occurrence of long lasting energetic flares, while the occurrence of flares and other phenomena with lower energies tend to follow the simple 11 year cycle. There is also an anticorrelation between the cycle ampli-

tude and the length of the rising phase, known as the Waldmeier effect (Waldmeier 1935, 1939).

There is no reason for stellar analogs of the solar cycle to be perfectly symmetric either, yet they are usually fitted with simple sinusoids, and not much focus has been paid to their shape. Reinhold et al. (2017) showed, that cycles derived from the variability of Kepler stars deviate from simple sinusoids, the average shape showing a sharp maximum and flattened minimum, and that this effect might have a temperature dependence, as it was weak for the coolest stars.

The solar cycle has been modelled with many different mathematical formulations accounting for their asymmetry (Nordemann 1992; Elling & Schwentek 1992; Hathaway et al. 1994; Volobuev 2009; Du 2011). Takalo & Mursula (2018) applied the Principal Component Analysis to the solar cycle and divided it into two components, an average cycle component, which always has the same shape, with varying period and amplitude, and one component varying from cycle to cycle.

One parameter which has been used to measure asymmetries of solar cycles is the skewness, a measure of asymmetry commonly used in statistics. Ramaswamy (1977) reported a relation between the ratio of the maximum sunspot number of the following cycle to the current cycle  $\mu$  and the skewness  $\gamma$  of the current cycle as

$$\gamma + 0.37\mu = 0.80. \quad (1)$$

Lantos (2006) improved the correlation by looking separately at even and odd cycles, and derived the following formulae:

$$\mu = \begin{cases} -2.1092\gamma + 1.9418, & \text{when the current cycle is even,} \\ -1.2552\gamma + 1.3570, & \text{when the current cycle is odd.} \end{cases} \quad (2)$$

Stellar cycles have, however, not been modelled as extensively. Garg et al. (2019) found the Waldmeier effect in stars from the Mount Wilson observatory data. They also studied stellar cycle asymmetries by fitting similar functions as has been done to the solar cycle, as well as calculating the skewness. Pipin & Kosovichev (2016) found from numerical mean-field simulations for solar-type stars, that magnetic cycles of a higher amplitude are more asymmetric, until at some amplitude the asymmetry gets saturated.

The commonly used methods to study stellar cycles are not capable of taking cycle asymmetries into account, since usually the cycles are assumed to have sinusoidal form. The Lomb-Scargle periodogram (Lomb 1976; Scargle 1982) is a commonly used method, but it assumes a strict periodicity, which is generally not the case in stellar activity cycles. The duration of the solar cycle, for instance, varies from about 8 years to 14 years. The use of quasi-periodic models allows the cycles not to be strictly periodic (Olsper et al. 2018). Here, we study each cycle individually to account for cycle-to-cycle differences in the duration and shape of the cycles.

## 2. Data

### 2.1. Mount Wilson data

We use the publicly available Ca II H&K S-index measurements from the Mount Wilson (MW) Observatory, a program started by Wilson (1978). The data set, including almost 2300 stars, was gathered between 1966 and 1995, with additional data for 35 stars extended to 2001. The S-index, defined as

$$S = \alpha \frac{H + K}{V + R}, \quad (3)$$

is a sensitive indicator of chromospheric magnetic activity (e.g. Egeland et al. 2017). Here  $H$  and  $K$  indicate flux integrated over narrow pass bands centered around the Ca II H and K line cores, and  $V$  and  $R$  are broad continuum bands on the violet and red sides of the Ca lines.  $\alpha$  is a calibration factor, which is determined for each night from standard lamp and standard star observations.

Baliunas et al. (1995) determined the periodicity of the MW stars with Lomb-Scargle periodograms, and divided the stars with cyclic variations into four different categories based on the False Alarm Probability (FAP), the probability that a peak as strong as the one observed would randomly occur in the Lomb-Scargle periodogram, assuming purely Gaussian noise. These categories are labeled as ‘excellent’, ‘good’, ‘fair’ and ‘poor’, corresponding to  $FAP \leq 10^{-9}$ ,  $10^{-9} < FAP \leq 10^{-5}$ ,  $10^{-5} < FAP \leq 10^{-2}$ , and  $10^{-2} < FAP \leq 10^{-1}$ , expressed in %, respectively. They, however, note that because of variations due to growth and decay of active regions, for instance, being non-Gaussian noise, the FAP should not be taken too literally.

Olsper et al. (2018) did a comparison between the cycle periods in Baliunas et al. (1995) and periods derived with quasi-periodic methods. They found that the results were similar for

the ‘excellent’ stars, while the resemblance weakens gradually for the ‘good’, ‘fair’ and ‘poor’ stars. Some of the differences, however, can be explained by their use of additional data from the extended 2001 data set, and a stronger significance level.

In our sample we have included all the stars defined as ‘excellent’ or ‘good’ by Baliunas et al. (1995), with the exception of HD 78366, HD 201092 and HD 156206, which are labeled as ‘good’. HD 78366 is left out because it is not clear where its minima are, since there are multiple ‘secondary minima’ in the data, and HD 201092 because its minimum around JD-2444000=2500 is very difficult to define; there seems to be a local maximum where the minimum should be according to the 11.7 year cycle reported by Baliunas et al. (1995). They found no secondary shorter cycle in HD 201092, although visual inspection would hint for that. HD 156206, on the other hand, does not have data to cover any cycle completely (from minimum to minimum). When these stars are left out, we have left a sample of 18 stars, all with fairly clear cycles. All the stars in our analysis have also been found to be cyclic by Olsper et al. (2018).

Most of our stars are main sequence stars, but there are also three giants included. The MW database also includes Ca II H&K measurements of the Sun. They have been done by measuring the Moon, as the lunar spectrum for the H&K lines is effectively just reflected sunlight. Since the Mount Wilson data includes only one full cycle for the Sun, we extended our data for the Sun by including Sacramento Peak (SP) Ca II K observations, which were scaled to the same level as the MW S-index as  $S_{SP} = 2.61K_{SP} - 0.0647$ , as was done by Olsper et al. (2018). This combined data set includes three full solar cycles.

The series for the Sun was even further extended back to 1907, including data from solar cycles 15 to 24, by Egeland et al. (2017), who also added Ca II K plage index measurements from the Kodaikanal Observatory in India and calibrated them to the MW scale. We use, however, only the data from MW and SP observatories, as was done in Olsper et al. (2018).

### 2.2. Sunspot numbers

To compare the stellar cycles to the solar cycle, we have also analysed sunspot data in addition to the solar chromospheric measurements. We compare the MW+SP data both to the classical Wolf Sunspot Number (WSN)<sup>1</sup>, and the Group Sunspot Number (GSN), recalibrated for different observers with the Active Day Fraction method by Willamo et al. (2017). Running back to 1610, the sunspot series is much longer than any time series of other active stars. We use the data for sunspot cycles 9-23, from 1843.5 to 2008.9, where multiple of these series (MW+SP, WSN and GSN) are available.

## 3. Methods

### 3.1. Defining times of minima and maxima

We have defined the times for minima and maxima of the stellar activity cycles individually for each cycle. To define the exact time we have fitted a parabola to the data around the minimum/maximum, with the interval of data included varying depending on the specifics of the cycle; if the cycle is very asymmetric around the minimum/maximum, only a short interval can be used when fitting a symmetric function, whereas with a poorly covered cycle a longer interval has to be used in order to get

<sup>1</sup> Source: WDC-SILSO, Royal Observatory of Belgium, Brussels; available at <http://www.sidc.be/silso/datafiles>

**Table 1.** Our sample of Mount Wilson stars.

Star	$n_{\text{cyc}}$	$\log R'_{\text{HK}}$	$T_{\text{eff}}$ [K]	$P_{\text{rot}}$ [d]	$P_{\text{cyc}}$ [yr]	$\langle\gamma\rangle$	$\sigma$	$\langle t_r \rangle / \langle t_d \rangle$	$n_{\text{bin}}$	FAP	MS/G	Data
HD 3651	1	-5.040	5280	37.0	15.06	0.368	...	0.594	10	G	MS	1995
HD 4628	2	-4.874	5014	37.14	8.21±0.41	0.096	0.145	0.905	10	E	MS	1995
HD 16160	1	-4.902	4762	48.58	12.18	0.074	...	1.023	10	E	MS	1995
HD 26965	2	-4.919	5196	38.65	10.34±0.07	0.076	0.131	0.864	10	E	MS	1995
HD 32147	1	-4.939	4703	33.7	10.40	0.127	...	0.758	10	E	MS	1995
HD 166620	1	-4.975	5007	42.1	15.33	0.146	...	0.723	10	E	MS	1995
HD 219834A	2	-5.098	5705	43.4	6.16±1.78	0.364	0.133	0.429	7	G	G	1995
HD 219834B	3	-4.919	5136	34.78	8.86±1.25	0.319	0.144	0.672	8	E	G	1995
Sun	3	-4.911	5780	26.09	10.90±1.23	0.394	0.161	0.625	10	E	MS	1995+SP
HD 10476	3	-4.962	5489	35.6	10.23±0.16	0.111	0.273	0.697	10	E	MS	2001
HD 81809	3	-4.940	5889	41.66	7.94±0.59	0.222	0.074	0.740	9	E	G	2001
HD 103095	3	-4.939	5265	34.03	6.94±0.42	0.202	0.133	0.917	10	E	MS	2001
HD 114710	3	-4.738	6098	11.99	5.44±0.34	0.107	0.463	0.676	8	G	MS	2001
HD 115404	2	-4.502	4976	18.03	10.62±1.99	0.158	0.028	0.742	10	G	MS	2001
HD 149661	6	-4.625	5265	20.76	4.68±1.25	-0.013	0.361	0.916	5	G	MS	2001
HD 152391	3	-4.469	5461	10.62	8.67±2.19	-0.040	0.342	0.959	8	E	MS	2001
HD 160346	4	-4.818	4897	32.0	7.15±0.26	0.109	0.071	0.772	7	E	MS	2001
HD 201091	4	-4.588	4177	35.54	7.05±0.70	-0.033	0.072	0.873	9	E	MS	2001

**Notes.** FAP = E/G (Excellent/Good) as defined by Baliunas et al. (1995). MS = main sequence star, G = giant.  $P_{\text{cyc}}$  is given with its standard deviation; thus there are no ‘error bars’ for stars with only one detected cycle.  $\gamma$  for the Sun has been calculated from solar cycles 21–23, which there is MW+SP data from, but to calculate  $\langle t_r \rangle / \langle t_d \rangle$  cycles 1–20 are also included, where all  $t_{\text{min}}$  and  $t_{\text{max}}$  are from the dates listed in Hathaway (2015). Source of  $T_{\text{eff}}$  for the Sun: Cox (2000).

enough data for a reliable fit. The times of minima and maxima defined by this method along with the intervals used are listed in the appendix (Table A.1). One cycle is then defined as the time between two consecutive minima.

For the dates of minima and maxima for the Sun we use the minimum and maximum value of the 13-month mean value of the sunspot number. This is a commonly used definition of solar minima (see e.g. Hathaway 2015). Note that this is the minimum of the sunspot number cycle, and the chromospheric emission need not necessarily be at its minimum at the same time – there are indeed differences of even several years in the timing of the solar minima between different activity indicators, such as the sunspot number, sunspot area and 10.7cm radio flux (Hathaway 2015). By using the same minima times for different solar activity indicators, however, the analysis done for the MW cycles of the Sun is comparable to that done for the sunspot cycles in Section 4.4. For other stars we have only MW data, so they are not necessarily directly comparable in that sense to the solar cycle.

### 3.2. Skewness

Skewness is a statistical measure of the asymmetry of a probability distribution, which has been used to measure asymmetries of solar cycles (Ramaswamy 1977; Lantos 2006; Du 2011).

The skewness  $\gamma$ , or third moment, of a set of data points  $x_i$  is defined as

$$\gamma = \frac{\sum_{i=1}^N (x_i - \bar{x})^3}{(N-1)\sigma_x^3}, \quad (4)$$

where  $N$  is the number of data points,  $\bar{x}$  the sample mean and  $\sigma_x$  the sample standard deviation. A positive skewness indicates a distribution leaning to the left, or in the case of a stellar cycle, a cycle with faster rise time and slower declining time, whereas a negative skewness indicates leaning to the right, or longer rise

time and shorter declining time. A symmetric distribution has  $\gamma = 0$ , although zero skewness does not necessarily mean the distribution is symmetric. For instance, a distribution with a long and thin tail on the other side and short but thick on the other, could also have  $\gamma = 0$ .

In order to calculate the skewness of an activity cycle, the cycle has to be transformed into a one-dimensional distribution. We have done this by dividing the cycle into ten bins of equal length, where the center of the bin is at  $t_{\text{bin}}$ . In the cases where there are too long gaps in the data and some bins would have no data points at all, we have reduced the number of bins into the largest number which still includes data points in each bin. Then we have calculated the mean value of the data points in each bin, and built the final distribution, emulating the cycle, by multiplying this mean value by 10 000 in order to get an integer value  $n$  from data with four decimals, and added  $n$  occurrences of  $t_{\text{bin}}$  to the distribution.

In order to compare the skewness of stellar cycles to the solar cycle, their zero-levels must be comparable. The sunspot cycle goes close to zero at solar minimum, whereas the S-index of active stars does not. To correct for this we have shifted all the bins of a cycle with a constant value, so that the bin with the smallest value goes to  $S_{\text{min}} = 0.001$  (corresponds to having the  $t_{\text{bin}}$  appear  $n = 10$  times in the distribution). This is done similarly to each cycle. An example of this kind of distributions emulating the cycles of HD 81809 is shown in Figure 1. We have done the same analysis, with the same shift of the zero-level, also to the sunspot cycle.

For each star, we have calculated the skewness for each cycle, and used the average of these as a measure of the average cycle asymmetry for this star.

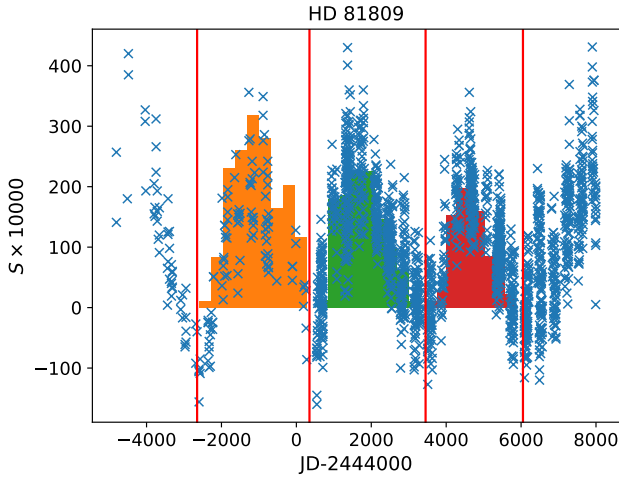


**Fig. 1.** Cycles of HD 81809. The crosses are the original calibrated MW data, and the histograms are the distributions built from these. Vertical lines show the times of minima, dividing the data set into three complete cycles. Note that the zero-levels of the histograms are defined individually for each one, but here they are plotted on the same level, so the correct, individual shifts for each cycle are lacking in the visualisation for simplicity. The value on the y-axis,  $S \times 10000$  (which has been shifted in the y-direction), equals the number of data points in a bin,  $n$ .

## 4. Results

### 4.1. Rise and decline times of cycles

A simple way to estimate the asymmetry of a cycle is to compare the duration of the rising phase and the declining phase of the cycle. In the Sun the rising phase is typically shorter.

For each star we calculated the ratio of the average duration for the rising phase  $\langle t_r \rangle$  and average duration of the declining phase  $\langle t_d \rangle$  of a cycle. Figure 2 shows the relation of this ratio to the average skewness of the star's cycles. Blue data points represent main sequence stars and red ones giants. The Sun is shown in yellow. As both are a measure of asymmetry, the more or less linear relation is expected. The values of  $\langle t_r \rangle / \langle t_d \rangle$  are also listed in Table 1.

For the calculation of the  $\langle t_r \rangle / \langle t_d \rangle$  parameter for the Sun we have used sunspot data for solar cycles 1-23 for better statistics. With any other stars the maximum number of cycles is six.

As the main measure of the cycle asymmetry we use the skewness of the cycle (see Sec. 4.2), but the correlation of the skewness and  $\langle t_r \rangle / \langle t_d \rangle$  confirms that both are usable parameters to measure cycle asymmetries. We calculated a Pearson correlation coefficient  $r = -0.78$  between these two parameters, which indicates a fairly strong negative correlation. Assuming linearity, we derived the relation between them as

$$\gamma = -0.68 \left[ \langle t_r \rangle / \langle t_d \rangle \right] + 0.69. \quad (5)$$

The times of minima and maxima are listed for each star in the appendix (Table A.1). Note that if available, we have used times of maxima of incomplete cycles to get better statistics. For instance, for HD 32147 there is only one complete cycle, but yet three times of maxima.

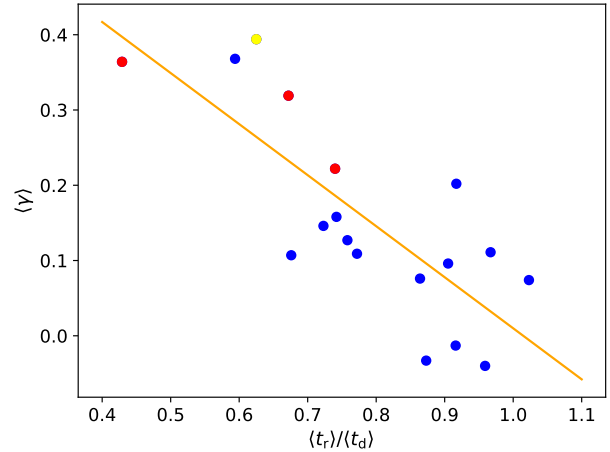


**Fig. 2.** The ratio of average rise time and average decline time versus average skewness. Blue dots represent main sequence stars, red ones giants. The Sun is shown in yellow. The continuous line shows the best linear fit.

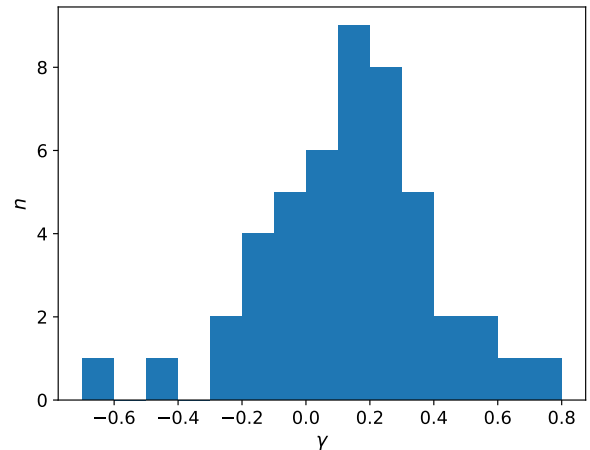


**Fig. 3.** The distribution of skews of all cycles of all stars.

### 4.2. Average skewness of MW cycles

The average skewness  $\langle \gamma \rangle$  for the cycles of each star and its standard deviation  $\sigma$  for those stars with multiple cycles is shown in Table 1.

Figure 3 shows the distribution of the skews of all cycles of all stars. We see that the majority (34 of a total number of 47 = 72%) of all cycles have a positive skew. The peak values are between 0.1 and 0.2. The Sun has a considerably high asymmetry, with a mean skew from MW+SP data of 0.394. Taking all 47 cycles into account, we get an average skewness 0.13, with a standard deviation 0.26.

We have compared the average skewness for each star to other stellar parameters; cycle period  $P_{\text{cyc}}$ , rotation period  $P_{\text{rot}}$ , effective surface temperature  $T_{\text{eff}}$  and activity index  $\log R'_{\text{HK}}$ , in Figures 4, 5, 6 and 7. The figures show the mean value and standard deviation of the variation of  $\gamma$  (and  $P_{\text{cyc}}$ ) for those stars with multiple cycles ( $\sigma$  and the standard deviation of  $P_{\text{cyc}}$  in Table 1). Values for  $P_{\text{rot}}$  and  $\log R'_{\text{HK}}$  are from Olsperg et al. (2018). The  $T_{\text{eff}}$  values are from Gaia DR2 (Gaia Collaboration et al. 2016, 2018; Andrae et al. 2018), except for the Sun.

In all figures, blue points represent main sequence stars and red ones giants. The Sun is shown in yellow. The three giants, as well as the Sun, have a considerably high skewness – actually, the Sun has the highest skewness of the stars in our sample. This is mainly due to the third cycle (solar cycle 23) being the second most positively skewed cycle of any star in our sample; solar cycles 21 and 22 are much more symmetric. Sunspot data also gives a much lower skewness for cycle 23 than MW+SP data (see Section 4.4). The value  $\langle t_r \rangle / \langle t_d \rangle = 0.625$  for the Sun, which has been calculated from sunspot cycles 1-23, is also a very asymmetric one, but there are two stars with even larger asymmetry in the rise and decline times. The skewness of the solar cycles from MW+SP data might thus be slightly biased due to an over-representation of very asymmetric cycles. It should be remembered, though, that the rise and decline times were calculated from sunspot data, which might behave differently than chromospheric data.

We calculated Pearson's correlation coefficients between  $\langle \gamma \rangle$  and the other parameters. These are shown in Table 2 along with their  $p$ -values. Between  $\langle \gamma \rangle$  and  $P_{\text{cyc}}$  or  $P_{\text{rot}}$  there is at best a very weak positive correlation. There might be a slightly stronger positive correlation between  $\langle \gamma \rangle$  and  $T_{\text{eff}}$ , but the most relevant is the negative correlation between  $\langle \gamma \rangle$  and  $\log R'_{\text{HK}}$  ( $r = -0.67$ ). The less active stars might thus have, in general, more asymmetric cycles. This would make sense since young, active stars are known to have more irregular cycles than older, less active stars (Baliunas et al. 1995). Irregular cycles could be skewed in either direction, and then be averaged close to symmetric cycles with zero skewness, if enough cycles are included. This correlation is, however, not clear. More data would need to be analysed before this could be claimed with some certainty. This differs from the simulated results of Pipin & Kosovichev (2016), who found stronger cycles to be more asymmetric in the regime of weak cycles in their mean-field simulations.

We have also compared our values for the average skewness to those of Garg et al. (2019), who studied the same data. This is shown in Figure 8. There are some large differences in the values. Our guess is that this is due to the definition of the zero-level or the binning, which are not described in detail in Garg et al. (2019), since that paper focused more on the Waldmeier effect than the cycle skews.

One source of uncertainty is the number of bins, which might affect the skewness of the cycle. In most cases the data is abundant and regular enough to allow us to divide it into 10 bins, but in some stars the number of bins has been reduced, in the worst case to 6. This is inevitable, since these data contains large gaps. The number of bins used for each star is listed in Table 1.

We tested the effect of the binning with the Sun, for which  $n_{\text{bin}} = 10$ , and average skewness  $\langle \gamma \rangle = 0.394$ . When reducing the number of bins to  $n_{\text{bin}} = 8$  we get  $\langle \gamma \rangle = 0.402$ , and with  $n_{\text{bin}} = 5$ ,  $\langle \gamma \rangle = 0.329$ . For stars with poorer data quality, this effect can be expected to be even larger. In any case it seems evident, that the stars with  $n_{\text{bin}} = 10$  are most comparable to each other.

Due to the gaps in the data, long cycles are probably more reliable than short ones, since the seasonal gaps affect a proportionally smaller part of the cycle, and the shape of the cycle can be identified with more certainty.

### 4.3. Average cycle shape

We also tried to combine all 47 individual cycles of all stars to an average cycle. The cycle amplitudes have been normalised with the same binning that was used in the calculation of  $\gamma$ , so that the lowest bin has the value 0 and the highest bin 1. We added

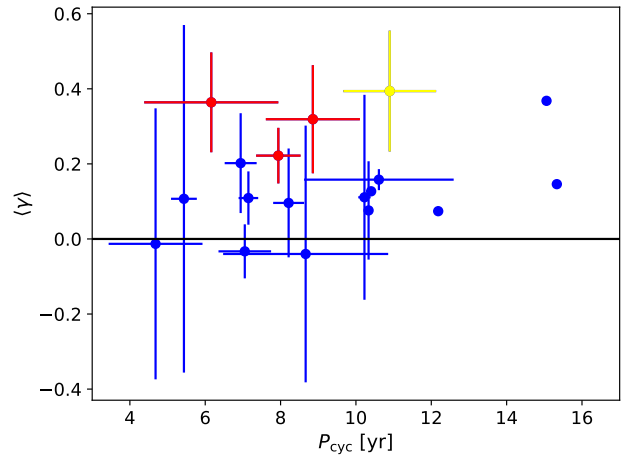


**Fig. 4.** The average skewness plotted against  $P_{\text{cyc}}$ . Blue dots represent main sequence stars, red ones giants. The Sun is shown in yellow. The error bars represent the cycle-to-cycle variations for stars with multiple cycles. The vertical line represents  $\gamma = 0$ .

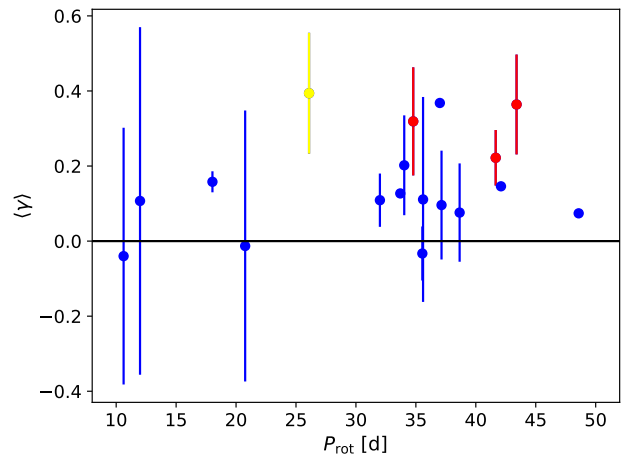


**Fig. 5.** Same as Figure 4 but for  $P_{\text{rot}}$ .

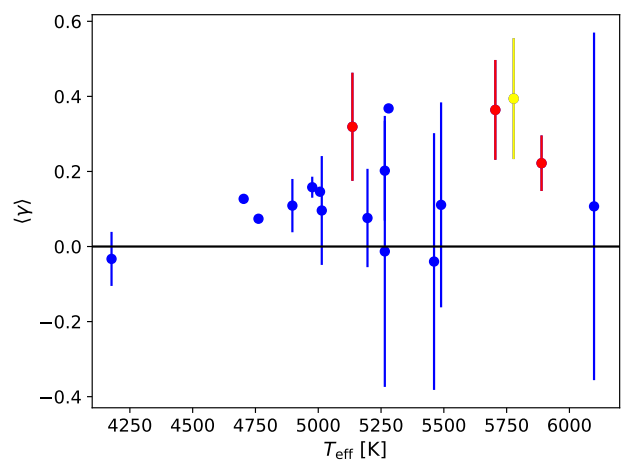


**Fig. 6.** Same as Figure 4 but for  $T_{\text{eff}}$ .

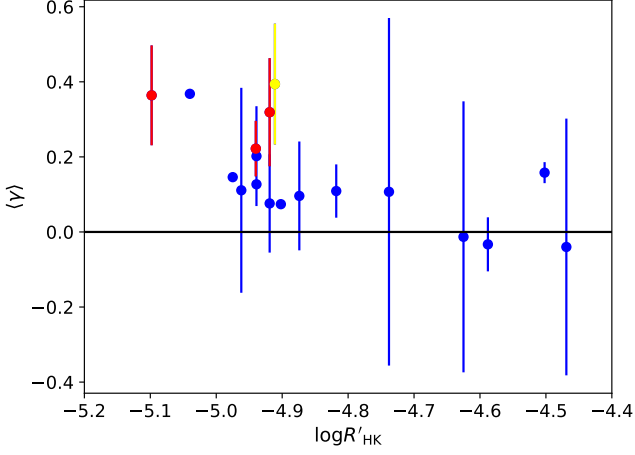


**Fig. 7.** Same as Figure 4 but for  $\log R'_{\text{HK}}$ .

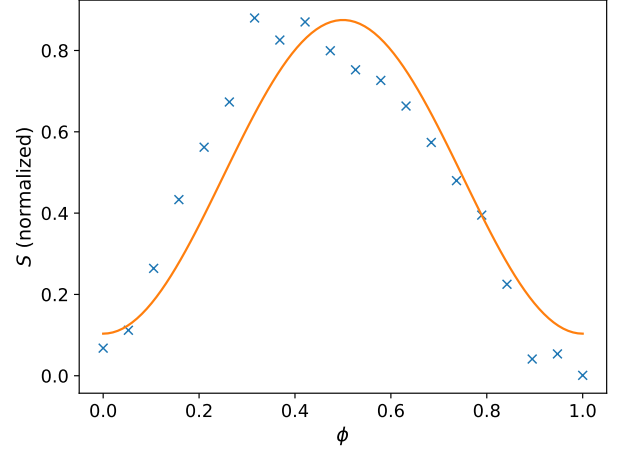


**Fig. 9.** All cycles phased and normalized together. The blue crosses show the resulting cycle, and the orange curve is a cosine fitted to the cycle.

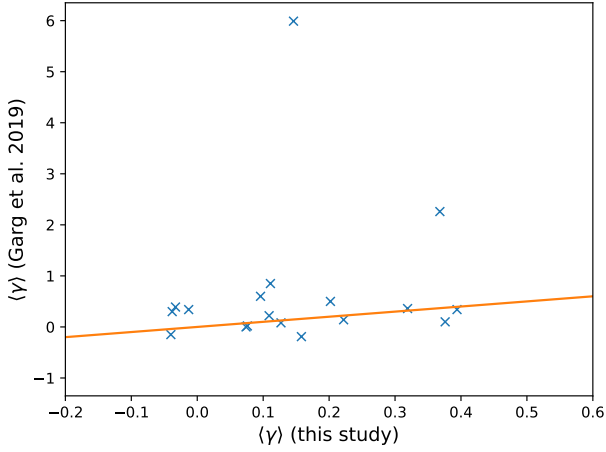


**Fig. 8.** Our average skewness for each star compared to that of Garg et al. (2019). The orange line is  $y=x$ , where these values would be equal.

**Table 2.** Correlation coefficients between  $\gamma$  and other parameters.

Parameter	Correlation coefficient	$p$ -value
$\langle t_r \rangle / \langle t_d \rangle$	-0.78	$1.3 \times 10^{-4}$
$P_{\text{cyc}}$	0.28	0.26
$P_{\text{rot}}$	0.29	0.24
$T_{\text{eff}}$	0.42	0.08
$\log R'_{\text{HK}}$	-0.67	$2.6 \times 10^{-3}$

all the data points from individual cycles, scaled between 0 and 1, to the combined cycle without any averaging. The scaling of individual cycles was, however, done with the mean values of the bins, to avoid extreme data points setting the scale for the cycles. The cycle duration was normalised to a phase between 0 and 1.

For the resulting average cycle,  $\gamma$  was calculated similarly as for individual cycles, except now we divided the data to 20 bins instead of 10, due to much more abundant data. We get the value for the skewness as  $\gamma = 0.078$ , which is slightly less than the average skewness for individual cycles.

We fitted a sinusoid of the form

$$S(\phi) = a \cos(2\pi\phi) + c, \quad (6)$$

to the averaged cycle with 20 data points (same as in the binning when calculating  $\gamma$ ). The cosine function has its minimum/maximum at 0, which is defined as the cycle minimum, so it is forced to the same phase as the cycle. The fitted cosine function, with the fitted parameters  $a = -0.386$  and  $c = 0.489$ , is shown in Figure 9. The fit is plausible, even though individual cycles can be very irregular. Quantitatively, we get the chi-squared statistics between the data points and the fitted sinusoid as  $\chi^2 = 11.43$ , and the  $p$ -value  $p = 0.91$ . The cosine curve is, however, not able to take into account the asymmetry, as the actual cycle rises to its maximum faster than the cosine. The best-fit cosine also has its maximum at a similar level as the actual average cycle, but its minimum is not as deep. This feature is different than the one noted by Reinhold et al. (2017) for Kepler stars, where the maximum was sharper, and the minimum flatter than the sine curve. They, however, used the amount of photometric variability as a proxy of magnetic activity. The variability should be highest around activity maximum, but the details of the cycles might still be different than those found from the S-index, and furthermore, the span of the Kepler data allow the detection of cycle periods only up to around 6 years.

In Figure 9 there might also be a hint of a double peak, as is commonly seen in the Sun, with the Gnevyshev gap in between. The feature is rather weak though, so from our data we can make no claim to the existence of double peaks and the Gnevyshev gap in other stars.

#### 4.4. Comparison to sunspot cycles

The stellar data can be compared to sunspot data. We have used the same method to calculate the skewness for monthly values of both the classical Wolf Sunspot Number (WSN) and the Group Sunspot Number (GSN) series. The GSN ignores individual spots and only counts the number of spot groups, which reduces observational errors and makes the old observations more reliable. We use the minimum values of the 13-month average number of sunspots as the times of solar minima: 1843.5,

**Table 3.** Skewness of the solar cycles.

#	MW+SP	WSN	GSN	Lantos (2006)	Du (2011)
9	...	0.114	-0.004	0.235	0.507
10	...	0.400	0.389	0.346	0.135
11	...	0.565	0.490	0.646	0.522
12	...	0.468	0.360	0.414	0.087
13	...	0.559	0.525	0.640	0.345
14	...	0.086	0.079	0.204	-0.074
15	...	0.339	0.342	0.314	0.327
16	...	0.180	0.191	0.262	0.020
17	...	0.417	0.425	0.299	0.122
18	...	0.294	0.264	0.273	0.162
19	...	0.629	0.607	0.581	0.299
20	...	0.375	0.232	0.330	0.043
21	0.338	0.134	0.158	0.299	0.116
22	0.231	0.357	...	0.419	0.164
23	0.614	0.282	...	...	0.300

1855.9, 1867.2, 1878.9, 1890.2, 1902.0, 1913.5, 1923.6, 1933.7, 1944.1, 1954.3, 1964.8, 1976.2, 1986.7, 1996.3 and 2008.9 (see e.g. Hathaway 2015).

Our values for the skewness of solar cycles 9 to 23 are shown in Table 3. We also compare our values to the skewness for the WSN published by other authors. Our values agree well with those of Lantos (2006), but not so with those of Du (2011). The skewness of the Group Sunspot Number is very similar to the skewness of the classical Wolf Sunspot Number.

There are some notable differences in the MW data and sunspot data. Especially for cycle 23 the MW data gives a very high skewness of  $\gamma = 0.614$ , whereas sunspot data gives  $\gamma = 0.282$ . If the MW cycles for the Sun are not comparable to the sunspot cycle, then cycles for other stars cannot be expected to be directly comparable to the sunspot cycle either.

## 5. Comparison to simulations

To compare our observational results to numerical simulations, we have used the direct numerical magnetohydrodynamic (MHD) simulations of convective dynamos in solar-like stars, described in Viviani et al. (2018), Warnecke (2018) and Warnecke & Käpylä (2019). Some of the simulation, presented in Viviani et al. (2018), are global MHD simulations, ranging between 0.7-1.0  $R$  in the radial direction, and only omitting the polar regions, modelling the star between latitudes  $-75^\circ$  to  $+75^\circ$ , and the full longitudinal range. A few of the runs in Viviani et al. (2018), and all the runs in Warnecke (2018) and Warnecke & Käpylä (2019) are wedges in the azimuthal direction, covering only the longitudes from 0 to  $\pi/2$ . These are labeled with the superscript ‘W’ in Table 4. A few of the global simulations are run in higher resolution. These are marked with the superscript ‘a’. The higher resolution runs are slightly more realistic, as they are more turbulent than their lower resolution counterparts. Besides comparing with the observed MW cycles, we also investigated whether the differing geometry of the simulation setup affects the results.

In all of these runs, turbulent convection under the influence of rotation generates differential rotation and large-scale dynamo action. As a result, dynamically significant dynamo modes at the system scale are generated and maintained by the flow.

The radial magnetic field at 0.98  $R$  is decomposed into spherical harmonics, where  $m = 0$  mode contains the axisymmetric part of the radial magnetic field,  $m = 1$  is the first non-

axisymmetric mode,  $m = 2$  the second, and so on. We have studied the evolution of the dominating dynamo mode in each simulation (found in Table 4 in Viviani et al. (2018)), which is  $m = 0$  or  $m = 1$  in all runs. In all the wedge runs  $m = 0$  is the dominating mode, containing most of the magnetic energy on large scales. We note here that a substantial amount of magnetic energy in all runs comes from the small-scale non-axisymmetric field, however for the comparison with observed cycles, only the large-scale magnetic field is relevant.

We chose the runs where cycles for the dominating mode could be defined for a closer study; this includes 20 runs in total. We chose only runs where more than one cycle could be identified, in order to get some estimate for the cycle-to-cycle variability. We point out that the simulations do not always produce strictly cyclic dynamo solutions, which is likely due to the competition of different dynamo modes in the simulated system. Hence, defining the cycle minima was more challenging from the models than from the MW data. Thus, the results may not be as reliable for the simulated data.

We built the distributions emulating the cycles similarly as for the MW data, by multiplying the value of each data point so that we get an integer number, and added this many occurrences of this time point to the distribution, and then fitted a parabola around the minimum to define its exact location. Then we calculated the skewness of each cycle similarly as with the MW data.

Figure 10 shows a histogram of the distribution of the skews of the simulated cycles, both for all cycles together, and including only the global runs or only the wedge runs. There is a visible difference between the global and wedge runs; while the histogram including all cycles is centered around zero, with a mean skewness 0.00 and standard deviation 0.32, the one including only the global runs has a mean skewness of 0.06 and standard deviation 0.31, and the one including only wedge runs has a mean of -0.06 and standard deviation 0.31. It would thus seem that global simulations produce more positively skewed cycles than wedge runs, although in both cases the cycle-to-cycle variation is large, as it is in real stars as well.

In both global and wedge runs, the deviation (0.31 in both cases) is larger than the difference between these (0.06 – (-0.06) = 0.12). To investigate if the difference is significant, we calculated additionally the standard error  $\sigma_{\langle\gamma\rangle}$  of the mean of the distribution:

$$\sigma_{\langle\gamma\rangle} = \frac{\sigma^2}{n}, \quad (7)$$

where  $n$  is the sample size. We get  $\sigma_{\langle\gamma\rangle, \text{global}} = 0.04$  and  $\sigma_{\langle\gamma\rangle, \text{wedge}} = 0.03$ . These are smaller than the difference, which indicates that it is significant and not noise caused by a small sample size. However, we note that for the global runs, a significantly large fraction of the cycles (14 of 48) are from the run K1, which has higher average skewness than most of the runs, and might induce a bias to the result. Nevertheless, we believe that the difference between the global and wedge runs, although small, is real.

The wedge assumption forces the dynamo to be axisymmetric, whereas in global simulations non-axisymmetry is also allowed. Hence, these simulations not only allow us to study the cycle asymmetry as a function of rotation or cycle period, but also study the effect of the degree of non-axisymmetry on it. By comparing skewness and axisymmetry of global simulations to observational data, one could try to deduce if cycles in real stars are dominated by axisymmetric or non-axisymmetric modes. Although the parameters in the simulations are still far-removed



from the real stellar conditions, in the future this may provide a diagnostic tool to further classify observational data into axisymmetric and non-axisymmetric modes.

Note, however, that even the global runs have a lower average skewness than the observed MW cycles. Assuming the observed chromospheric emission to be directly proportional to the magnetic field strength, it is thus plausible to believe, that some ingredient is still missing in the simulations, which causes the asymmetry in the observed cycles. The simulations are, for example, still in a parameter regime that is too mildly turbulent, and they do not, include realistic photospheres or chromospheres. The other alternative is that cycles are more symmetric for more rapidly rotating stars (for which there is a weak correlation in the MW data). In this case the different parameter regime of the observations and simulations might explain their difference, since the rotation was much faster in most of the simulated runs than in the observed stars.

Similarly to the observational data, we also compared the mean skewness of each run to other stellar parameters. Table 4 shows the mean skewness of all these runs, and the rotation rate of the simulated star, normalised to the solar rotation rate  $\tilde{\Omega}$ . The rotation rate is transformed to rotation period by  $P_{\text{rot}} = P_{\odot}/\tilde{\Omega}$ , where  $P_{\odot} = 26.09$  d is the rotational period of the Sun.  $\langle\gamma\rangle$  is plotted against  $P_{\text{rot}}$  in Figure 11, and against  $P_{\text{cyc}}$  in Figure 12. Global and wedge simulations are separated from each other in the figures, as are the higher resolution global runs. We calculated Pearson correlation coefficients between  $\langle\gamma\rangle$  and  $P_{\text{rot}}$ , and  $\langle\gamma\rangle$  and  $P_{\text{cyc}}$ , for all simulations together, and separately for the global and wedge runs. These are shown in Table 5. The strongest correlation is  $r = -0.57$  for  $P_{\text{rot}}$  for the global simulations, although this is fairly weak. Also, the correlation is positive for the wedge runs. For  $P_{\text{cyc}}$  the correlations are even weaker. We draw no other conclusions from this, besides the lack of strong correlations between cycle asymmetry and other parameters, as was the case with observed cycles as well.

Note that the cycle period, which we defined from the times of minima, was determined differently by Viviani et al. (2018), who counted how many times the mean magnetic energy level is crossed, and Warnecke (2018), who determined the period with power spectra.

It must also be noted that the rotation rate, although the most relevant parameter, is not the only parameter varied between the simulations. Other input parameters changed between the runs are the grid resolution, the fluid-, subgrid-scale- and magnetic Prandtl numbers, the Taylor number and the Rayleigh number. We have not, however, analysed how these affect the cycle asymmetry, since these parameters are not known for real, individual stars.

Table 6 summarizes the main features of the simulated cycles, both including all cycles, and when separating the global and wedge runs.

## 6. Conclusions

We draw the following conclusions from our study:

- A fast rise and slower decline is common for stellar activity cycles.
- The Sun has particularly asymmetric cycles.
- More active stars might have less asymmetric cycles, but the correlation between the skewness and other parameters is mostly unclear.

- Individual cycles might have very irregular shapes, but the average cycle shape is fairly well represented with a sinusoid. The average cycle still reaches its maximum before the sinusoid, due to its asymmetry.
- The chromospheric and sunspot cycles do not have exactly the same shape. This means that MW cycles for other stars can probably not be directly compared to the sunspot cycle.
- The numerically simulated cycles, with shorter rotation periods than the observed real stars, have on average more symmetric cycles, with a distribution in the skewness values centered very close to zero. Perhaps the simulations are missing something which makes the cycles asymmetric in real stars. This can indicate that the physics still not captured by these models, such as the missing photosphere and chromosphere, is crucial for creating the cycle asymmetries. Other explanations for this could be a difference in the cycles between slow and fast rotators, for which there is some support from the weak correlation between the skewness and the rotation period, and the stronger anticorrelation between the skewness and  $\log R'_{\text{HK}}$  in the MW data.
- The simulation geometry affects the asymmetry of the simulated cycles, with the wedge simulations having on average more negatively skewed cycles than the global simulations.

*Acknowledgements.* The HK\_Project\_v1995\_NSO data derive from the Mount Wilson Observatory HK Project, which was supported by both public and private funds through the Carnegie Observatories, the Mount Wilson Institute, and the Harvard-Smithsonian Center for Astrophysics starting in 1966 and continuing for over 36 years. These data are the result of the dedicated work of O. Wilson, A. Vaughan, G. Preston, D. Duncan, S. Baliunas, and many others. This work has made use of data from the European Space Agency (ESA) mission *Gaia* (<https://www.cosmos.esa.int/gaia>), processed by the *Gaia* Data Processing and Analysis Consortium (DPAC, <https://www.cosmos.esa.int/web/gaia/dpac/consortium>). Funding for the DPAC has been provided by national institutions, in particular the institutions participating in the *Gaia* Multilateral Agreement. TW acknowledges the financial support from the Alfred Kordelein Foundation, and thanks Angie Breimann, who had a similar idea as the one of this paper. Our discussion during the BCool meeting in Exeter was most fruitful. TH acknowledges the financial support from the Academy of Finland for the project SOLSTICE (decision No. 324161). MJK and NO acknowledge the support of the Academy of Finland ReSoLVE Centre of Excellence (grant No. 307411). This project has received funding from the European Research Council under the European Union's Horizon 2020 research and innovation programme (project "UniSDyn", grant agreement n:o 818665). MV was enrolled in the International Max Planck Research School for Solar System Science at the University of Göttingen.

## References

- Andrae, R., Fouesneau, M., Creevey, O., et al. 2018, *A&A*, 616, A8  
 Baliunas, S. L., Donahue, R. A., Soon, W. H., et al. 1995, *ApJ*, 438, 269  
 Cox, A. N. 2000, *Allen's astrophysical quantities*  
 Deng, L. H., Xiang, Y. Y., Qu, Z. N., & An, J. M. 2016, *AJ*, 151, 70  
 Du, Z. 2011, *Sol. Phys.*, 273, 231  
 Egeland, R., Soon, W., Baliunas, S., et al. 2017, *ApJ*, 835, 25  
 Elling, W. & Schwentek, H. 1992, *Sol. Phys.*, 137, 155  
 Feminella, F. & Storini, M. 1997, *A&A*, 322, 311  
 Gaia Collaboration, Brown, A. G. A., Vallenari, A., et al. 2018, *A&A*, 616, A1  
 Gaia Collaboration, Prusti, T., de Bruijne, J. H. J., et al. 2016, *A&A*, 595, A1  
 Garg, S., Karak, B. B., Egeland, R., Soon, W., & Baliunas, S. 2019, *ApJ*, 886, 132  
 Gnevyshev, M. N. 1963, *Soviet Ast.*, 7, 311  
 Gnevyshev, M. N. 1967, *Sol. Phys.*, 1, 107  
 Gnevyshev, M. N. 1977, *Sol. Phys.*, 51, 175  
 Hathaway, D. H. 2015, *Living Reviews in Solar Physics*, 12, 4  
 Hathaway, D. H., Wilson, R. M., & Reichmann, E. J. 1994, *Sol. Phys.*, 151, 177  
 Lantos, P. 2006, *Sol. Phys.*, 236, 199  
 Lomb, N. R. 1976, *Ap&SS*, 39, 447  
 Newton, H. W. & Milsom, A. S. 1955, *MNRAS*, 115, 398  
 Nikbaksh, S., Tanskanen, E. I., Käpylä, M. J., & Hackman, T. 2019, *A&A*, 629, A45  
 Nordemann, D. J. R. 1992, *Sol. Phys.*, 141, 199



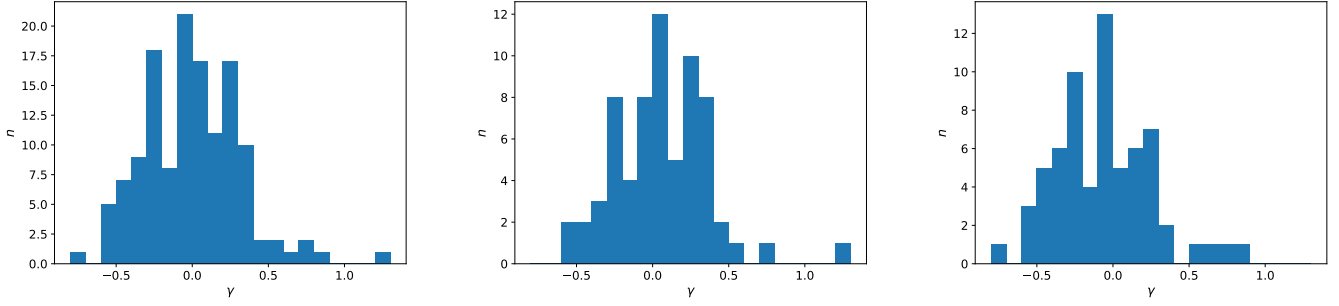


**Fig. 10.** The distribution of skews of individual cycles for all the runs (left), only the global runs (center) and only the wedge runs (right).

**Table 4.** Skewness of the simulated cycles. The runs are named as in the corresponding reference.

Run	$n_{\text{cyc}}$	$\langle\gamma\rangle$	$\sigma$	$\tilde{\Omega}$	$P_{\text{rot}}$ [d]	$P_{\text{cyc}}$ [yr]	G/W	Reference
A1	2	-0.323	0.239	1.0	26.09	$3.20 \pm 0.25$	G	Viviani et al. (2018)
C2	7	0.061	0.230	1.8	14.49	$5.02 \pm 2.14$	G	Viviani et al. (2018)
E	2	0.179	0.199	2.9	9.00	$13.41 \pm 2.63$	G	Viviani et al. (2018)
F1	4	0.106	0.124	4.3	6.07	$4.14 \pm 1.65$	G	Viviani et al. (2018)
G <sup>a</sup>	4	0.012	0.325	4.9	5.32	$7.69 \pm 3.12$	G	Viviani et al. (2018)
H <sup>a</sup>	6	-0.173	0.208	7.8	3.34	$2.60 \pm 0.62$	G	Viviani et al. (2018)
J	2	-0.090	0.127	14.5	1.80	$5.14 \pm 0.71$	G	Viviani et al. (2018)
K1	14	0.209	0.458	21.4	1.22	$1.85 \pm 0.58$	G	Viviani et al. (2018)
L <sup>a</sup>	3	0.303	0.148	23.3	1.12	$3.16 \pm 0.62$	G	Viviani et al. (2018)
M	4	0.050	0.122	28.5	0.92	$6.73 \pm 0.68$	G	Viviani et al. (2018)
M2	10	0.162	0.376	2.0	13.05	$4.09 \pm 1.30$	W	Warnecke (2018)
M2.5	5	0.047	0.474	2.5	10.44	$4.13 \pm 0.90$	W	Warnecke (2018)
M3	3	-0.258	0.413	3.0	8.70	$7.22 \pm 1.88$	W	Warnecke (2018)
M5	13	-0.165	0.266	5.0	5.22	$2.17 \pm 0.35$	W	Warnecke (2018)
M7	12	-0.092	0.160	7.0	3.73	$2.75 \pm 0.78$	W	Warnecke (2018)
M10	13	-0.163	0.219	10.0	2.61	$2.61 \pm 0.73$	W	Warnecke (2018)
M15	4	-0.076	0.082	15.0	1.74	$5.68 \pm 2.27$	W	Warnecke (2018)
J <sup>W</sup>	9	0.050	0.216	15.5	1.68	$4.70 \pm 1.97$	W	Viviani et al. (2018)
M30	6	0.093	0.230	30.0	0.87	$5.58 \pm 2.87$	W	Warnecke & Käpylä (2019)
M <sup>W</sup>	10	0.030	0.204	31.0	0.84	$4.15 \pm 2.10$	W	Viviani et al. (2018)

**Notes.** The G/W column divides the runs into global (G) and wedge (W) runs. The high resolution runs are named with the superscript *a*.

**Table 5.** Correlation coefficients between  $\langle\gamma\rangle$  and other parameters in the simulated cycles.

Parameter	Correlation coefficient	<i>p</i> -value
$P_{\text{rot,all}}$	-0.32	0.17
$P_{\text{rot,global}}$	-0.57	0.09
$P_{\text{rot,wedge}}$	0.12	0.75
$P_{\text{cyc,all}}$	0.19	0.11
$P_{\text{cyc,global}}$	0.21	0.59
$P_{\text{cyc,wedge}}$	$3.6 \times 10^{-3}$	0.99

Reinhold, T., Cameron, R. H., & Gizon, L. 2017, A&A, 603, A52  
Scargle, J. D. 1982, ApJ, 263, 835  
Takalo, J. & Mursula, K. 2018, A&A, 620, 100  
Viviani, M., Warnecke, J., Käpylä, M. J., et al. 2018, A&A, 616, A160  
Volobuev, D. M. 2009, Sol. Phys., 258, 319  
Waldmeier, M. 1935, Astronomische Mitteilungen der Eidgenössischen Sternwarte Zurich, 14, 105  
Waldmeier, M. 1939, Astronomische Mitteilungen der Eidgenössischen Sternwarte Zurich, 14, 470  
Warnecke, J. 2018, A&A, 616, A72  
Warnecke, J. & Käpylä, M. J. 2019, arXiv e-prints, arXiv:1910.06776  
Willamo, T., Usoskin, I. G., & Kovaltsov, G. A. 2017, A&A, 601, A109  
Wilson, O. C. 1978, ApJ, 226, 379

**Table 6.** The average skewness and its standard deviation of the observed and simulated cycles.

Parameter	MW	All simulated runs	Global	Wedge
$\langle\gamma\rangle$	0.11	0.00	0.06	-0.06
$\sigma$	0.28	0.32	0.31	0.31

Norton, A. A. & Gallagher, J. C. 2010, Sol. Phys., 261, 193  
Olsper, N., Lehtinen, J. J., Käpylä, M. J., Pelt, J., & Grigorievskiy, A. 2018, A&A, 619, A6  
Pipin, V. V. & Kosovichev, A. G. 2016, ApJ, 823, 133  
Ramaswamy, G. 1977, Nature, 265, 713

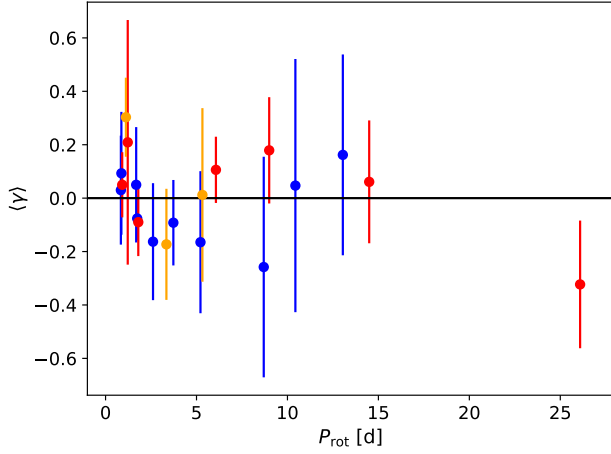


**Fig. 11.** The mean skewness of the simulated cycles as a function of  $P_{\text{rot}}$ . The error bars represent the standard deviation of the cycles in the run. Global runs are shown in red, with the high resolution runs in orange, and the wedge runs in blue. The horizontal line represents  $\gamma = 0$ .

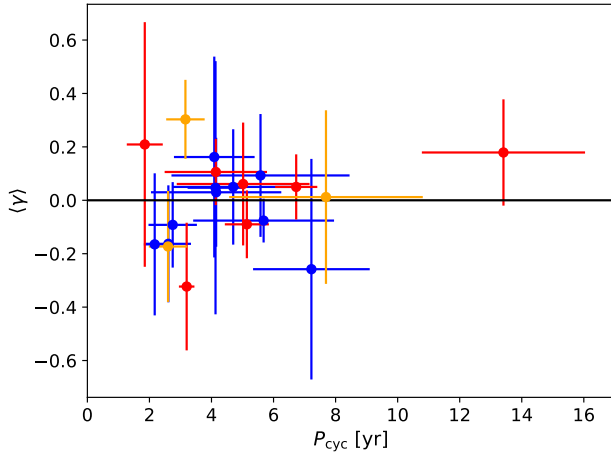


**Fig. 12.** Same as Figure 11 but for  $P_{\text{cyc}}$ .

## **Appendix A: Minima and maxima of individual MW cycles**

**Table A.1.** Times of minima and maxima for the MW stars and the time intervals used to derive these as upper and lower index, and period and skewness for each cycle.

HD	# <sub>cyc</sub>	$t_{\min}$	$t_{\max}$	$P_{\text{cyc}}$ [yr]	$\gamma$
3651	1	-2600 <sup>-1000</sup> <sub>-4000</sub> , 2900 <sup>5000</sup> <sub>1000</sub>	-550 <sup>500</sup> <sub>-1500</sub>	15.06	0.368
4628	1	-2450 <sup>-1500</sup> <sub>-3500</sub> , 400 <sup>1300</sup> <sub>-500</sub>	-1000 <sup>0</sup> <sub>-2000</sub>	7.80	-0.049
4628	2	400, 3550 <sup>4700</sup> <sub>2500</sub>	1800 <sup>2800</sup> <sub>800</sub>	8.62	0.242
16160	1	-900 <sup>500</sup> <sub>-2000</sub> , 3550 <sup>500</sup> <sub>2500</sub>	1350 <sup>2300</sup> <sub>500</sub>	12.18	0.074
26965	1	-2050 <sup>-1000</sup> <sub>-3200</sub> , 1700 <sup>2500</sup> <sub>1000</sub>	-300 <sup>1300</sup> <sub>-1700</sub>	10.27	-0.055
26965	2	1700, 5500 <sup>6000</sup> <sub>4800</sub>	3450 <sup>4500</sup> <sub>2500</sub>	10.40	0.207
32147	1	-1050 <sup>-200</sup> <sub>-1800</sub> , 2750 <sup>3700</sup> <sub>2000</sub>	-3150 <sup>-2200</sup> <sub>-4300</sub> , 300 <sup>1100</sup> <sub>-600</sub> , 4850 <sup>5500</sup> <sub>4200</sub>	10.40	0.127
166620	1	-2200 <sup>-800</sup> <sub>-3300</sub> , 3400 <sup>4500</sup> <sub>2200</sub>	150 <sup>1000</sup> <sub>-1500</sub>	15.33	0.146
219834A	1	150 <sup>1000</sup> <sub>-800</sub> , 3050 <sup>3600</sup> <sub>2200</sub>	1000 <sup>1800</sup> <sub>300</sub>	7.94	0.231
219834A	2	3050, 4650 <sup>5500</sup> <sub>4000</sub>	3550 <sup>4500</sup> <sub>3000</sub>	4.38	0.496
219834B	1	-3950 <sup>-3000</sup> <sub>-4500</sub> , -500 <sup>1000</sup> <sub>-1500</sub>	-2700 <sup>-1900</sup> <sub>-4000</sub>	9.45	0.521
219834B	2	-500, 3150 <sup>3600</sup> <sub>2600</sub>	1100 <sup>1800</sup> <sub>300</sub>	9.99	0.197
219834B	3	3150, 5750 <sup>6000</sup> <sub>5000</sub>	4200 <sup>4700</sup> <sub>3600</sub>	7.12	0.238
Sun	1	-1150, 2650	200	10.40	0.338
Sun	2	2650, 6200	3700	9.72	0.231
Sun	3	6200, 10800	7650	12.59	0.614
10476	3	-2900 <sup>-2100</sup> <sub>-3600</sub> , 900 <sup>1400</sup> <sub>400</sub>	-1350 <sup>-500</sup> <sub>-2200</sub>	10.40	0.109
10476	2	900, 4550 <sup>5100</sup> <sub>3700</sub>	2100 <sup>2600</sup> <sub>1500</sub>	9.99	0.446
10476	3	4550, 8300 <sup>8500</sup> <sub>7500</sub>	6400 <sup>7000</sup> <sub>5800</sub>	10.27	-0.224
81809	1	-2650 <sup>-2100</sup> <sub>-3200</sub> , 350 <sup>1000</sup> <sub>-500</sub>	-1250 <sup>-500</sup> <sub>-2000</sub>	8.21	0.128
81809	2	350, 3450 <sup>4000</sup> <sub>3000</sub>	1600 <sup>2300</sup> <sub>900</sub>	8.49	0.310
81809	3	3450, 6050 <sup>6700</sup> <sub>5200</sub>	4500 <sup>5200</sup> <sub>4100</sub>	7.12	0.228
103095	1	-1700 <sup>-1000</sup> <sub>-2400</sub> , 750 <sup>1600</sup> <sub>-300</sub>	-600 <sup>300</sup> <sub>-1300</sub>	6.71	0.260
103095	2	750, 3500 <sup>3800</sup> <sub>3100</sub>	2100 <sup>2700</sup> <sub>1600</sub>	7.53	0.018
103095	3	3500, 5900 <sup>6800</sup> <sub>5000</sub>	4600 <sup>5300</sup> <sub>3800</sub> , 7300 <sup>7800</sup> <sub>6800</sub>	6.57	0.328
114710	1	1200 <sup>1800</sup> <sub>500</sub> , 3350 <sup>3800</sup> <sub>2700</sub>	1750 <sup>2300</sup> <sub>1300</sub>	5.89	0.761
114710	2	3350, 5300 <sup>5800</sup> <sub>4700</sub>	4300 <sup>4900</sup> <sub>3500</sub>	5.34	-0.248
114710	3	5300, 7150 <sup>8100</sup> <sub>6400</sub>	6200 <sup>6700</sup> <sub>5700</sub>	5.07	-0.193
115404	1	-1100 <sup>-300</sup> <sub>-2000</sub> , 3500 <sup>4000</sup> <sub>3200</sub>	400 <sup>1500</sup> <sub>-800</sub>	12.59	0.130
115404	2	3500, 6650 <sup>7100</sup> <sub>6100</sub>	5300 <sup>6000</sup> <sub>4600</sub>	8.62	0.186
149661	1	-3350 <sup>-2800</sup> <sub>-3800</sub> , -1700 <sup>-1300</sup> <sub>-2300</sub>	-2400 <sup>-1800</sup> <sub>-3000</sub>	4.52	0.006
149661	2	-1700, -400 <sup>200</sup> <sub>-1200</sub>	-1300 <sup>-500</sup> <sub>-1900</sub>	3.56	0.524
149661	3	-400, 1300 <sup>1800</sup> <sub>800</sub>	400 <sup>1300</sup> <sub>-300</sub>	4.65	-0.123
149661	4	1300, 2500 <sup>3100</sup> <sub>2100</sub>	2000 <sup>2800</sup> <sub>1300</sub>	3.29	-0.114
149661	5	2500, 5100 <sup>5700</sup> <sub>4200</sub>	3400 <sup>4000</sup> <sub>2500</sub>	7.12	0.268
149661	6	5100, 6900 <sup>7400</sup> <sub>6500</sub>	6250 <sup>6800</sup> <sub>5800</sub>	4.93	-0.638
152391	1	-1800 <sup>-500</sup> <sub>-3200</sub> , 2100 <sup>2800</sup> <sub>1600</sub>	200 <sup>800</sup> <sub>-500</sub>	10.68	-0.460
152391	2	2100, 5650 <sup>6100</sup> <sub>5000</sub>	4050 <sup>4900</sup> <sub>3200</sub>	9.72	-0.038
152391	3	5650, 7700 <sup>8200</sup> <sub>7200</sub>	6350 <sup>6800</sup> <sub>5800</sub>	5.61	0.379
160346	1	-3750 <sup>-3000</sup> <sub>-4100</sub> , -1100 <sup>-500</sup> <sub>-1600</sub>	-2700 <sup>-2000</sup> <sub>-3300</sub>	7.26	0.008
160346	2	-1100, 1400 <sup>2000</sup> <sub>1000</sub>	150 <sup>700</sup> <sub>-500</sub>	6.84	0.178
160346	3	1400, 3950 <sup>4600</sup> <sub>3200</sub>	2350 <sup>2800</sup> <sub>1800</sub>	6.98	0.077
160346	4	3950, 6700 <sup>7200</sup> <sub>6200</sub>	5250 <sup>5700</sup> <sub>4700</sub>	7.53	0.175
201091	1	-3400 <sup>-3100</sup> <sub>-3800</sub> , -850 <sup>-400</sup> <sub>-1400</sub>	-2300 <sup>-1800</sup> <sub>-2800</sub>	6.98	-0.085
201091	2	-850, 2150 <sup>2800</sup> <sub>1800</sub>	400 <sup>1000</sup> <sub>0</sub>	8.21	-0.004
201091	3	2150, 4500 <sup>5100</sup> <sub>4000</sub>	3400 <sup>4000</sup> <sub>2500</sub>	6.43	0.071
201091	4	4500, 6900 <sup>7600</sup> <sub>6400</sub>	5700 <sup>6500</sup> <sub>5000</sub>	6.57	-0.113

**Notes.** [ $t_{\min/\max}$ ]=JD-2444000.  $t_{\min}$  and  $t_{\max}$  for the Sun are from Hathaway (2015). Intervals used in the fitting of minima are only listed once for each minimum. With HD 32147 and HD 103095 the additional maxima have been used in to increase statistics in the calculation of  $\langle t_r \rangle / \langle t_d \rangle$ .